Final Project

(Saunon Malekshahi)

Abstract

This paper introduces a design for a rotorcraft blade capable of operating within the Martian atmosphere. Characterized by the performance requirements needed for operability in the cold, low-density atmosphere, the three-bladed rotorcraft propeller is designed around uniform, span-wise thrust loading so as to minimize lifting moments across the rotorblades. The Selig S1223 airfoil was selected, whose design conditions for C_L and flow separation was first confirmed. Based off of initial design constraints for thrust, rotor disk area, and sectional angle of attack, blade geometry parameters for chord, twist, and cross-sectional length were established. Lastly, the cross-sectional contributions of thrust, normal, and viscous drag forces were determined, along with those of the sectional twisting and bending moments.

1 Introduction

Rotorcraft are vehicles that use rotary wings to principally generate their lift. A series of airfoil blades attached to a central hub form a rotor, whose spanwise twist and chord is tapered to meet certain performance requirements.

The human endeavor for vertical flight dates back several centuries, as far back as 400 CE [1], with variants of rotary-wing kites in China; de Vinci's helical airscrew; and in 1936 with Focke Achgelis' first successful helicopter. Centuries of experimentation, coupled with the advances in rotorcraft dynamics of the previous decades, have enabled helicopters to flourish as a viable means of transportation.

More recently, NASA has been exploring development of a wide range of terrestrial spacecraft as part of its Mars Exploration Program. In particular, the concept for a rotorcraft has been made possible by the surge of commercial spaceflight and NASA's research efforts in understanding the fluid properties of the Martian atmosphere. The NASA Mars Helicopter, which will be accompanying the 2020 Rover on its mission to the red planet, is the latest development to come from the initiative. As such, the study of rotorcraft dynamics on other planets is now within the relevant scope of fluid and aerodynamic behavior.

2 Overview

The Vortex Panel Method formulation derived in the previous projects is used to verify the design lift criteria of $C_L = 2$ at $\alpha = 5$, and whether flow separation occurs at $\frac{x}{c} = 0.25$ for $\alpha = 5$. These results are confirmed and presented in Figure 1.

A series of fixed design constraints were established to fully parametrize design of the blade. These are presented in the following table.

Rotorblade Parameters	**Value**
Total Hovering Mass	$1kg$
Rotor Disk Loading	$T = mg_{Mars} = 3.71N$
Sectional Thrust	$t = \frac{\frac{T}{3}}{N} = 0.0124N$
Disk Area	$A_d = 1.5m^2$
Hover Induced Velocity	$V_h = \sqrt{T/2\rho A_d} = 8.7916m/s$
Rotational Velocity	$\Omega = 174.65rad/s$
Solidity (3 Blades)	$\sigma = 0.1$
Blade Root-to-Tip Radius Ratio	$\frac{r_r}{r_t} = 0.25$
Section Angle of Attack (w.r.t. V_h)	$\alpha = 5$

Table 1: Rotorblade Design Fixed Parameters

By leapfrogging from the stipulated constraints, blade geometry parameters were then determined at discrete blade sections extending radially outward. A mesh of $N = 100$ elements was used for this analysis, so as to construct the radially-dependent flow and geometry factors.

$$\Delta b = 0.75 * r_{tip}/N \tag{1}$$

Finite, spanwise rotor elements are given by (1). Sectional relative blade velocity $V_r(r)$ was then determined along with the sectional twist angle $\beta(r)$.

$$V_r(r) = \sqrt{(\Omega r)^2 + V_h^2} \tag{2}$$

$$\beta(r) = \frac{V_h}{\Omega r} \tag{3}$$

The VPM is run again on the airfoil to obtain the pressure distributions C_P across all the panels S_j. This is used to construct the sectional normal and thrust force contributions, along with sectional twist and bending moments. Ultimately, these parameters are used to determine the chord variance.

$$C_{Fx} = \sum_{i=1}^{N} -C_{Pi} S_{ji} \sin(\theta_i + \pi/2) \tag{4}$$

$$C_{Fy} = \sum_{i=1}^{N} -C_{Pi} S_{ji} \cos(\theta_i + \pi/2) \tag{5}$$

The lift and drag twisting moment coefficients are given by (4) and (5), respectively. The contribution of drag-induced twist is neglected in this analysis, as drag-induced moments are small for thin airfoils. A rotation about the section angle of attack $\alpha = 5$ is conducted to shift the lift and drag components from the local airfoil frame to the relative velocity frame.

$$\begin{bmatrix} \cos\alpha & \sin\alpha \\ -\sin\alpha & \cos\alpha \end{bmatrix} \begin{bmatrix} C_{Fx} \\ C_{Fy} \end{bmatrix} = \begin{bmatrix} C_D \\ C_L \end{bmatrix}$$

This operation effectively yields us with the cross-sectional drag and lift coefficients. A second rotation is applied around $\beta(r)$ to rotate the drag and lift coefficients into the frame of the rotor plane.

$$\begin{bmatrix} \cos\beta(r) & \sin\beta(r) \\ -\sin\beta(r) & \cos\beta(r) \end{bmatrix} \begin{bmatrix} C_D \\ C_L \end{bmatrix} = \begin{bmatrix} C_N \\ C_T \end{bmatrix}$$

From this operation we obtain the cross-sectional normal and thrust coefficients. Finally, the sectional chord variation $c(r)$ is solved for, using the previously obtained parameters.

$$C_T(r) = \frac{t}{\frac{1}{2}\rho V_r(r)^2 \Delta b c(r)} \tag{6}$$

These geometric parameters effectively establish the shape of the rotor blades. Analysis is then carried out on sectional viscous drag, net viscous drag torque, along with twisting and bending moment distributions. Sectional viscous drag $C_{D,v}(r)$ is determined at discrete elements by flow past a flat plate formulation. First, the Reynold's number $Re(r)$ is determined by

$$Re(r) = \frac{V_r(r)c(r)}{\nu} \tag{7}$$

which is then factored into

$$C_{D,v}(r) = 2(0.664)Re(r)^{-1/2} \tag{8}$$

(8) is used to determine the net viscous drag torque acting on the blade.

$$\tau = \sum_{r=r_{root}}^{r_{tip}} c(r)(\frac{1}{2}\rho V_r(r)^2)(\Delta b c(r))r \tag{9}$$

Lastly, bending and twisting moment distributions across the span of the blade are determined.

$$C_{m,y} = C_T(r)r \tag{10}$$

$$C_{m,tw} = \sum_{i=1}^{N} c(r)(x_i - 0.25)C_{Fi}(\frac{1}{2}\rho V_r(r)^2 \Delta b c(r) \tag{11}$$

The rotor blade performance parameters and geometry are plotted and presented in the appendix.

3 Discussion

By inspection of the chord and blade twist variation, it is immediately observable that the resulting geometry is consistently accounting for the uniform thrust loading requirement. This makes sense; the relative velocity experienced by the blade tips are far greater than those inward the root. As a result, the blade elements nearest the root must capitalize on the lower velocity by augmenting chord length.

Furthermore, what is notable is the significantly low viscous drag acting along the span of the rotor blade. This is consistent with the low-density, nearly inviscid atmospheric conditions on Mars, and supports the need for a high rotor rotational velocity to produce sustained lift (i.e. $\Omega = 174.65 rad/s = 1667.78 RPM$, compared to an Apache Helicopter, $\Omega_{Apache} = 289 RPM$).

4 Conclusion

As rotorcraft and aircraft development cross into different fluid realms, endeavors such as a Mars helicopter highlight the design limitations of an Earth-based system. There exist inherent challenges with optimally suiting geometries to conform to the surrounding fluid environment; this is an adverse "curve-fitting" approach. Specifically, achieving rotations up to 2000RPM (or more) would require development of a new, certified helicopter-grade engine. These limitations, among others, may point to the need to conceive vehicle and propulsive designs from an unprecedented standpoint.

5 Appendix

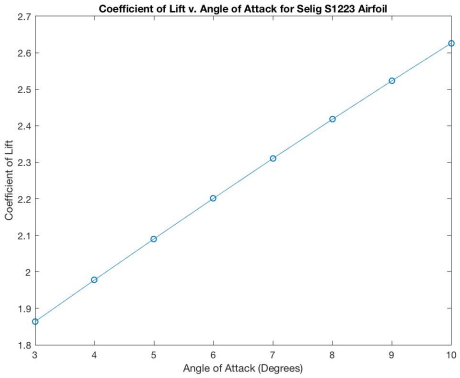

(a) C_L vs. α

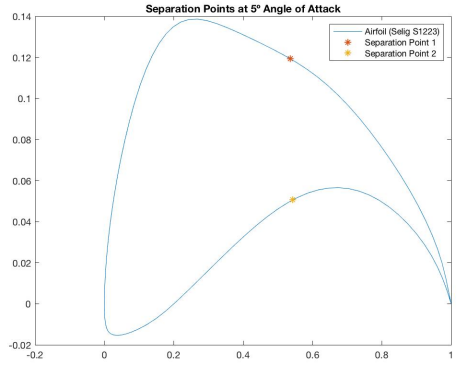

(b) Separation Points at $\alpha = 5$

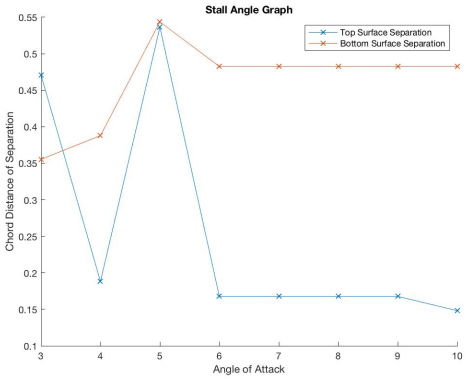

(c) Separation Points for $\alpha = 3 - 10$

Figure 1: Selig S1223 Design Criteria Analysis

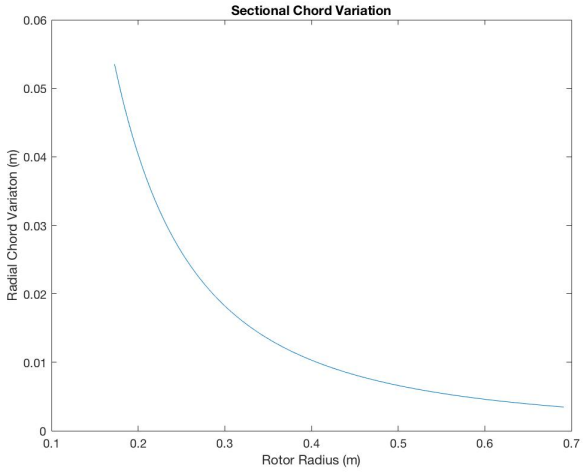

Figure 2: Sectional Chord Variation $c(r)$

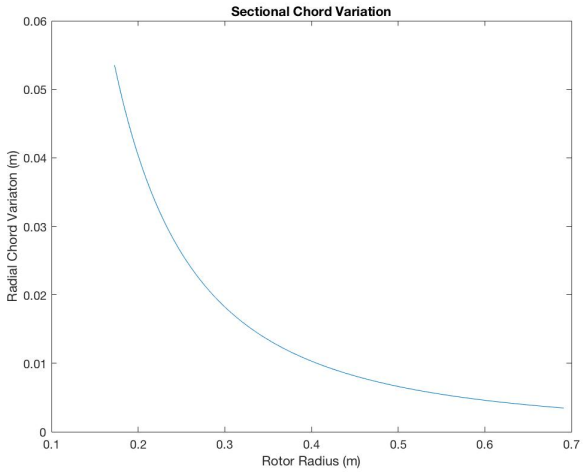

Figure 3: Sectional Blade Twist Angle Variation $\beta(r)$

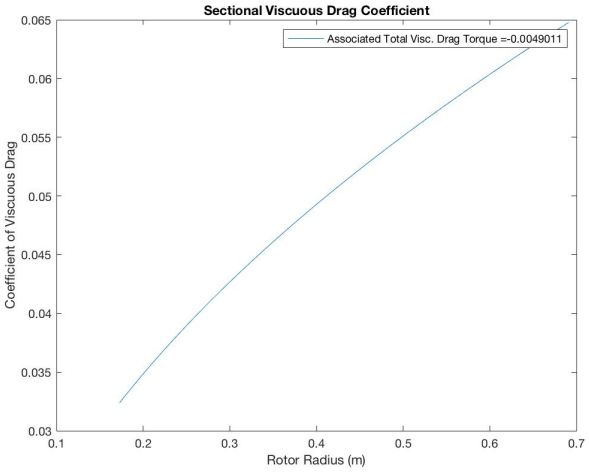

Figure 4: Sectional Viscous Drag Coefficient Variation $C_{D,v}(r)$

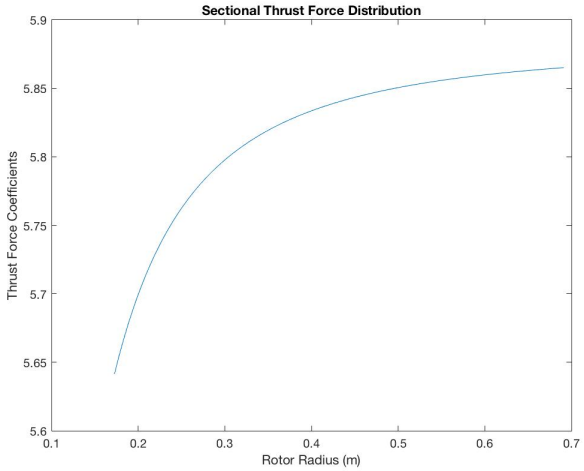

Figure 5: Sectional Thrust Distribution, $C_t(r)$

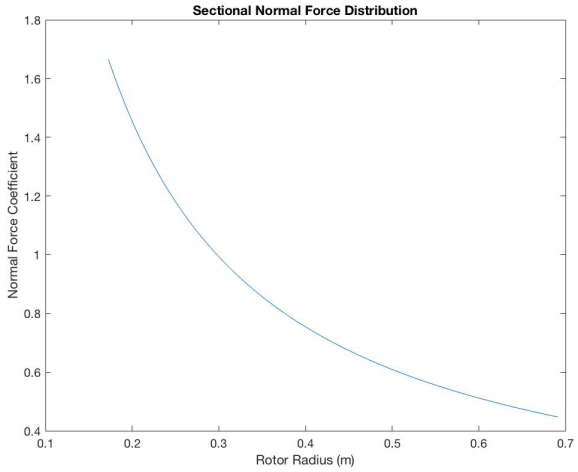

Figure 6: Sectional Normal Distribution, $C_n(r)$

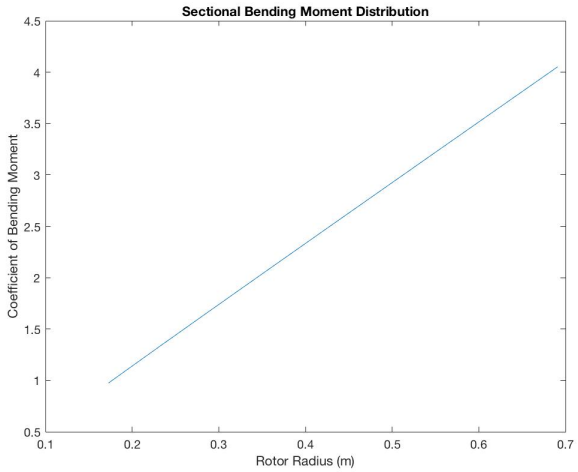

Figure 7: Distribution of Spanwise Blade Bending Moments

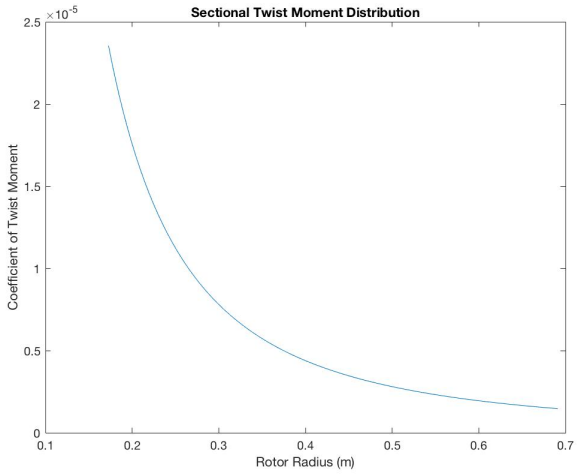

Figure 8: Distribution of Spanwise Blade Twisting Moments

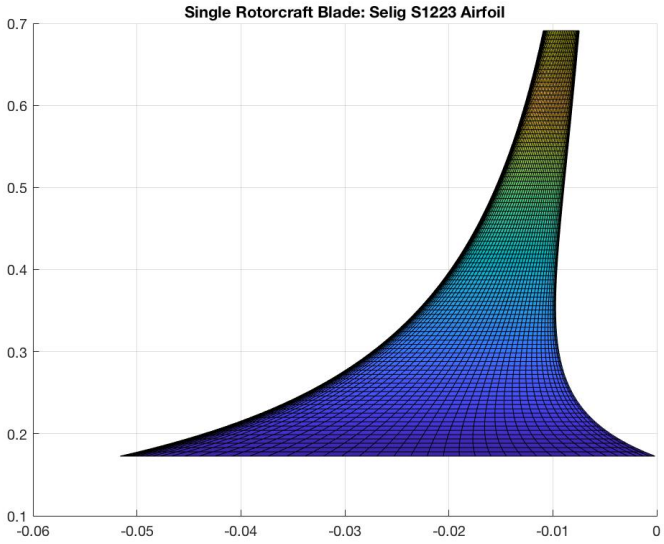

(a) Rotor Blade Top View

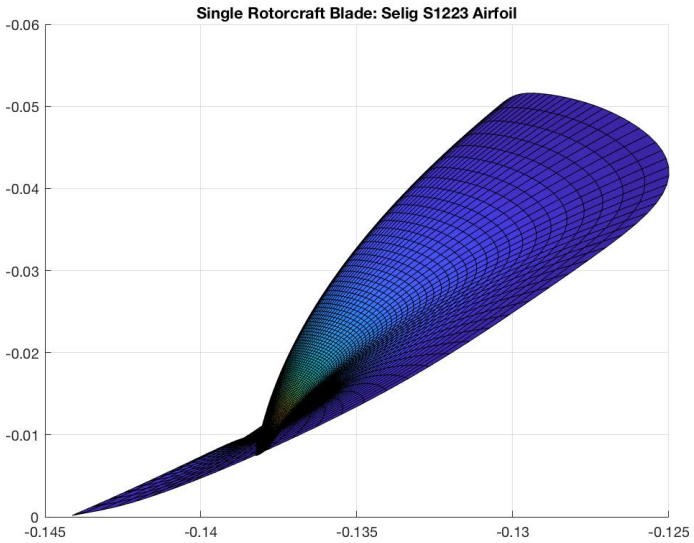

(b) Rotor Blade Side View

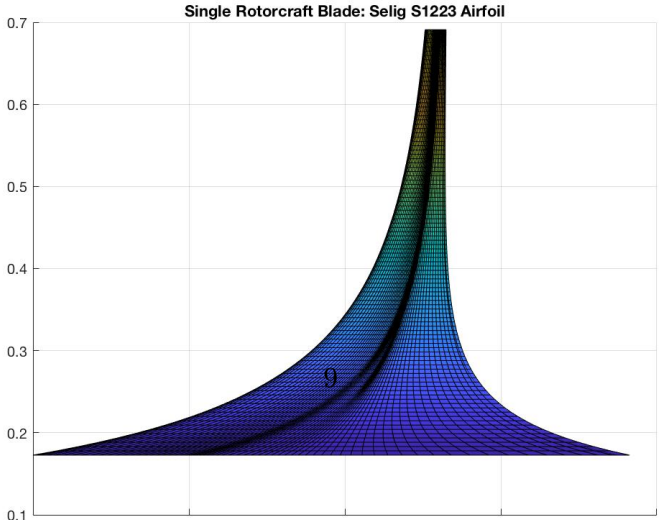

6 References

References

[1] Walter James Boyne. Helicopter, Jun 2018.